We are IntechOpen, the world's leading publisher of Open Access books Built by scientists, for scientists

4,800
Open access books available

122,000
International authors and editors

135M
Downloads

Our authors are among the

154
Countries delivered to

TOP 1%
most cited scientists

12.2%
Contributors from top 500 universities

CLARIVATE ANALYTICS BOOK CITATION INDEX INDEXED

WEB OF SCIENCE™

Selection of our books indexed in the Book Citation Index in Web of Science™ Core Collection (BKCI)

Interested in publishing with us?
Contact book.department@intechopen.com

Numbers displayed above are based on latest data collected.
For more information visit www.intechopen.com

Chapter 3

Performance Characteristics of Modelled Tri-Wing Solar Chimney and Adaptation to Wood Drying

R. S. Bello, C. N. Ezebuilo, K. A. Eke and
T. A. Adegbulugbe

Additional information is available at the end of the chapter

http://dx.doi.org/10.5772/59423

1. Introduction

Chimneys have been used for ventilation and space conditioning for centuries particularly in Europe by the Romans as well as in the Middle East and north east by Persians [1]. The concept of solar energy utilization in the chimney was proposed in 1960 by Trombe and Michel at the C.N.R.S. laboratory in France [2]. In the early stages of solar chimney development, it was exclusively used for space heating, but presently its use has been diversified both for heating and building ventilation technology, like passive solar applications [3, 4], low thermal applications [5] and thermogenerators [6] which can be used for comforts in buildings, as well as for agriculture [7]. Other uses of solar energy processes are classified as thermal processes, which include distillation of seawater to produce potable water, refrigeration and air conditioning, power production by solar-generated steam, cooking, water heating and the use of solar furnaces to produce high temperatures for experimental studies [6]. Solar energy technologies such as photovoltaic cells, thermoelectric cells, thermionic cells, thermo-emissive cells, etc. are also being used in small-scale applications in commercial projects.

The first mathematical modelling for the solar chimney (Trombe wall) design was given by Bansal et al., 1993 who also reported the concept of increasing the airflow by increasing solar irradiation. This theoretical study also reported an air change per hour with change in the coefficient of fluid (air) discharge. Ong, (2001) reported the mathematical model of a conventional vertical chimney which operates under the natural convention condition where the temperature of the air inside the chimney is warmer than outside. Shiv, et al., (2013) presented solar chimney as a solar air heater whose position may be vertical or horizontal, and according to the position, it could be regarded a part of a wall (in the form of Trombe wall) or a roof solar collector [10]. The roof solar chimney is the most convenient and mature technology used for buoyancy-driven natural ventilation systems [1, 12, 13].

2. Working principle of solar chimney

The solar chimney is one of the technologies which work on the principle of buoyancy, where air is heated through the greenhouse effect generated by solar radiation (heat energy) at low costs. The solar chimney is a passive solar ventilation system (non-mechanical) that can be installed on roofs or in walls. The heat is transferred through the convective cooling principle based on the fact that hot air rises upward; these chimneys reduce unwanted heat during the day by displacing interior (warm) air with exterior (cool) air. Solar chimneys are mainly made of a black, hollow thermal mass with an opening at the top as an exit for the hot air. The air in the room exits from the top of the chimney. The process can also be reversed for room heating. The configuration of a typical Trombe wall solar chimney is shown in Figure 1.

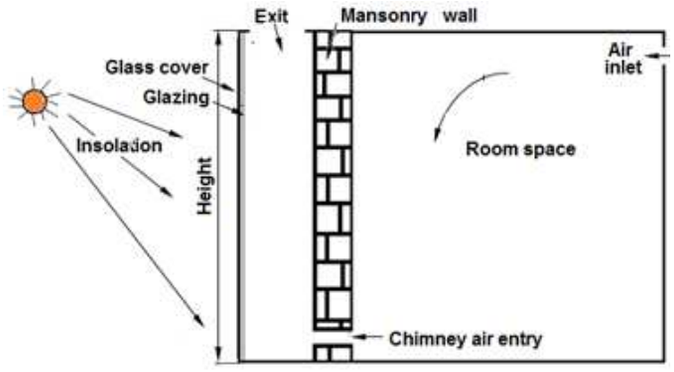

Figure 1. Solar chimney used in building ventilation

3. Classification of solar chimney

A detailed review of the solar chimney identified the following classifications:

1. The solar chimney can be classified according to its position as (i) a vertical solar chimney or (ii) an inclined solar chimney.
2. The solar chimney for building ventilation is classified according to its position as (i) a wall solar chimney, or Trombe wall; (ii) a roof solar chimney; and (iii) an integrated wall and roof solar chimney.
3. The solar chimney performance depends on the glazing, either single glazing, double glazing or triple glazing. The ventilation rate mainly depends on the height of the solar chimney, so it is one of the bases for classification, as (i) small height, (ii) medium height and (iv) large height.
4. The solar chimney is also classified according to its use for (i) building ventilation (circulation), (ii) building heating (dwelling), (iii) air dryer (crop dryer) and (iv) power generation.

http://dx.doi.org/10.5772/59423

5. The classification of the solar chimney is also associated with the cooling and heating of buildings. It means that the solar chimney can be classified based on integrated approaches as (i) integrated with evaporative cooling system, (ii) integrated with earth-air-tunnel heat exchanger and (iii) integrated with absorption and adsorption cooling.
6. The solar-radiation-receiving area is covered with a glass cover; the small radiations entering the system through glass cover as well as large wavelength radiation exiting from glass cover should be minimum to generate maximum greenhouse effect,. The greenhouse effect is associated with solar radiation and the number of glazing. The solar chimney is classified according to the number of glazing as (i) single glazing and (ii) multi-glazing.

3.1. Solar chimney performance

Ekechukwu and Norton, (1997) analyzed the performance of solar chimney for natural circulation of solar energy dryers and reported that the simple air heater increases ventilation up to some extent but not sufficiently. Mathur and Mathur, (2006) also experimentally analyzed the window-sized solar chimney and found a better summer performance of the inclined roof solar chimney. They studied the effects of various performance parameters like chimney width and height and solar radiation.

The performance of the solar chimney can be improved by using glazing, increasing height and air gap, integrating the Trombe wall with a roof solar collector (single pass and double pass) and selecting an appropriate inclination angle. Lee and Strand, (2009) investigated the effect of these parameters along with chimney height, air gap and potential for different climatic conditions. Hirunlabh, (1999) investigated the effect of glazing on the performance of the solar chimney and found that double glazing is a suitable option as compared to single and triple glazing. Gan, (1998) analyzed the glazed solar chimney experimentally and the data validated by simulation in a passively cooled building (PCB) and found that the airflow rate should be increased up to 17% in summer by using double glazing.

The solar chimney has the following merits: no mechanical parts, low maintenance, no electrical consumption, no global warming effects, no pollution and can be used for both heating and cooling. Its only demerit is the increase in the cost of building [11].

3.2. Buoyancy in solar chimney

Buoyant forces result due to free convection heat transfer from the solar heated plate of the collector to the surrounding air. This results into upward motion of the fluid (air) against gravity due to change in air density arising from the process. Since air buoyancy is proportional to the temperature difference, reduced heat losses and increased heat transfer rates will give a better performance. The atmospheric density decreases with increase in altitude; this effect restrains the height of chimney because the density of the air exiting from the chimney must always be less than the ambient air density [9]. If the density of air from the chimney is equal to the ambient air density, there will be stagnation in the flow, and if the chimney air density is further lessen, then the air backflow against the ambient will result, thereby resulting in local heat losses, which may stall buoyancy-induced forces. To cushion this effect, some form of insolation is needed at the upper section of the chimney.

3.3. Project objective

The object of this analysis is to investigate the drying effect of buoyant airflow created by solar heating of a tri-wing collector in the chimney and its application in the drying of agricultural products. To ensure effective design of the solar chimney, solar parametric equations were utilized to model drying conditions such as the maximum differential between the ambient air density and chimney outlet air density and its effects on agricultural drying applications. The air density depends on the temperature; hence, it also implies that the maximum difference between the chimney air temperature and the ambient temperature should give the best chimney performance. A complete analysis of the tri-wing collector with a mathematical model is cumbersome because of its distinct features compared to an ordinary flat-plate model; however, a comparison of its performance and effectiveness with experimental design data carried out with high-precision apparatus and equipment offers a realistic solution.

4. Experimental setup

A properly designed solar chimney should aim at maximum heat transfer from the received insolation to air as well as be of optimum height so as not to exceed the height at which the chimney air temperature cools to that of the ambient air. However, short chimney heights could result in low pressure heads. Based on these facts, the configuration of the experimental solar chimney was made 5.3m high and 1.64m in diameter for a hollow cylindrical channel of glass glazing. The walls of the chimney were made as smooth as possible to reduce pressure losses due to wall friction.

The absorbing surface (collector) is a tri-wing multi-flapped selective absorber plate draped inside the glazed glass. This chimney is mounted above the room space (drying chamber) through which dry air passes (Figure 2).

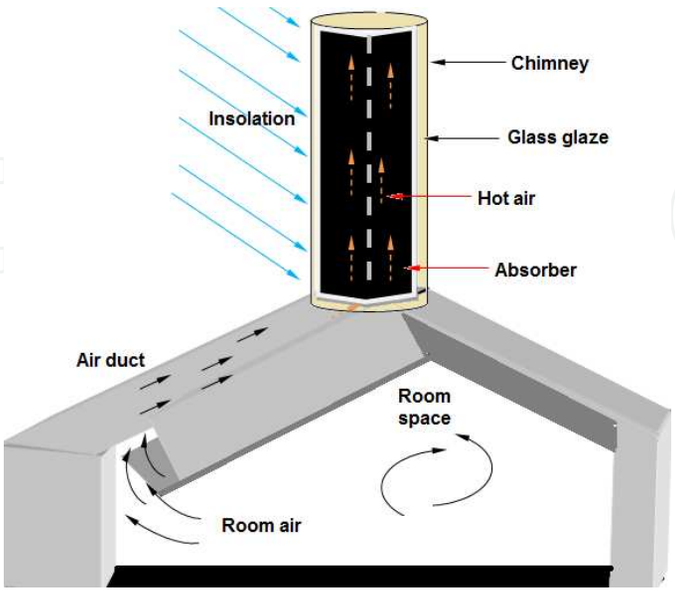

Figure 2. Schematic diagram of solar chimney

http://dx.doi.org/10.5772/59423

4.1. Features of solar chimney

Some distinguishing features of this solar chimney include the following:

1. Cylindrical glazing: The cylindrical glazing of the chimney makes the analysis of the transmittance-absorptance product differs from that of a flat cover glazing.
2. Multi-flapped absorber plate : The multi-flapped absorber plate of other existing chimney-type collectors has unequal insolation for each flap, and shadows are cast on adjacent flaps.
3. Back insulation: No back insulation is provided in the collector. This feature is an added heat transfer advantage in that absorbed radiation is transferred from both sides of the plate to air with elimination of back insulation losses.

4.2. Collector configuration solar insolation

The absorber plate is made of cast iron to eliminate heat flow resistance due to welds and a well-polished selective plate with high solar absorptance, α, of 0.9. The three wings of the collector were separated equiangularly at 120° and denoted as 1, 2, 3, with wing 2 aligned at zero azimuth angle while wings 1 and 3 at 120° azimuths, respectively. This implies that the collector is oriented such that wing 2 is aligned with geographic south. This symmetrical arrangement makes the thermal analysis easy on the configuration (Figure 3).

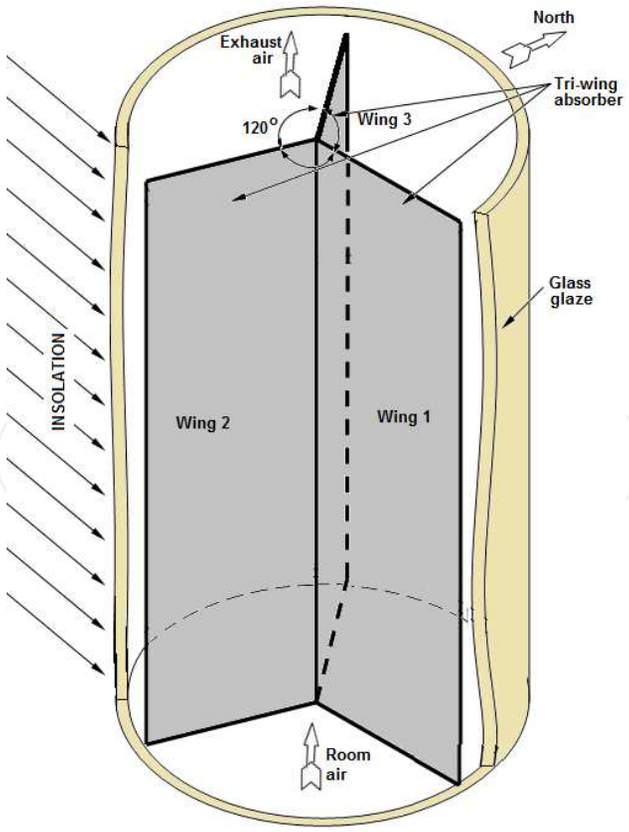

Figure 3. Schematic diagram of a solar chimney system

At any point in time, all the collector wings receive an equal amount of diffuse solar radiation but uneven direct beam radiation due to the shadow cast on adjacent wings. At any position of the sun, only two wings of the collector receive full-area direct radiation. For instance, when the sun is between the azimuth of east and south, wings 1 and 2 receive full-area radiation at different incident angles, while wing 3 receives partial-area direct radiation due to the shadow of wing 2 cast on it. The case is reverse when the sun is between the azimuths of south and west, the critical time of changeover. When the sun is over the azimuth of 0°, wings 1 and 3 receive full-area direct radiation at different incident angles and wing 2 receives partial direct radiation. This only happens intermittently (Figure 4).

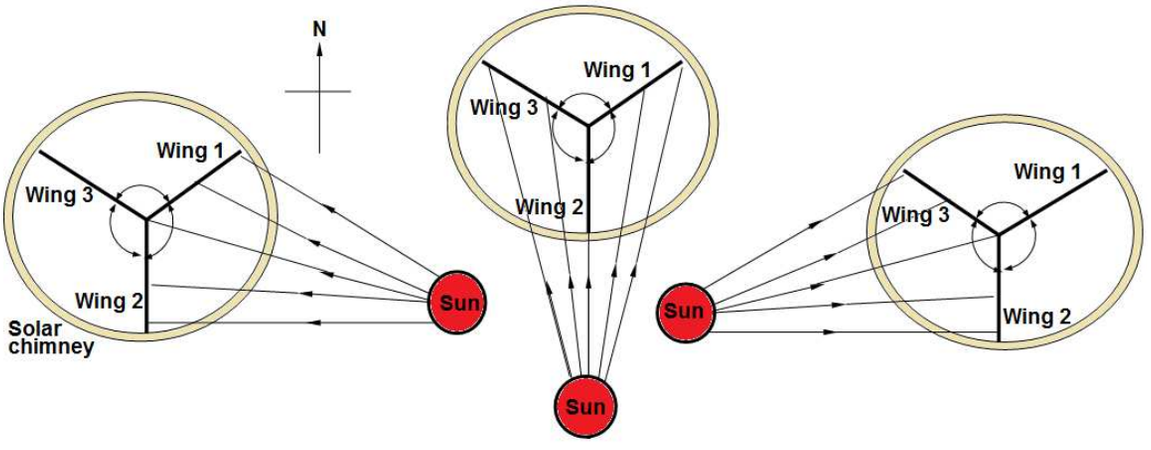

Figure 4. Azimuth positions of the solar insolation with respect to the three absorber surfaces

The shading of the wings must be accounted for to evaluate the actual direct beam radiation absorbed by each wing so that average radiation absorbed by the whole collector can be deduced. To achieve this, a factor of direct beam area ratio, (∀), is introduced. This is the ratio of the area of a wing of the collector lightened by direct beam radiation to the area of the whole wing. The shape of the lightened region of the shadowed wing is always triangular depending on the zenith angle of the sun. At a smaller zenith angle, a larger portion of the farther wing is lightened, while a smaller portion is lightened at a higher zenith angle.

To evaluate the absorbed solar radiation on a tilted surface with respect to a horizontal surface, the values of the ratio of beam radiation, R_b, on the vertical surface of the collector to that on the horizontal surface are required. The values of R_b will be evaluated using equation (1) for wings 1, 2 and 3 at the surface azimuth angle given as –120°, 0° and 120°, respectively:

$$R_b = \frac{\text{Cos}\theta}{\text{Cos}\theta_z} \tag{1}$$

where θ is the incident angle of radiation given as

http://dx.doi.org/10.5772/59423

$$\mathrm{Cos}\,\theta = -\sin\delta\ cos\varphi\ \cos\gamma + \cos\delta\ \sin\varphi\ cos\gamma\ cos\omega + \cos\delta\ \sin\gamma\ \sin\omega \tag{2}$$

This is expressed for each of the wings in terms of ω. The values of zenith angle θ_z in each wing are evaluated at the midpoint of an hourly time interval from 7.00am to 5.00pm of solar time. The zenith angle is expressed as [19]

$$\theta_z = \mathrm{Cos}^{-o}\left[\cos\delta\cos\varphi\ \cos\omega + \sin\delta\ \sin\varphi\right] \tag{3}$$

5. System heat transfer mechanism in the model

A complete heat transfer analysis of the multi-flapped collector involves a complex differential analysis of the absorbed radiation due to shadows and transient heat flow of flaps at different potentials. A complete analysis with a mathematical model is cumbersome because of its distinct features compared to an ordinary flat-plate model.

To overcome this, it was assumed that the collector absorber material is made of a highly conductive metal such that heat due to absorbed radiation is evenly distributed in all the collector flaps. This implies that solar radiation incident on the collector is such that there is no temperature gradient anywhere in the collector (i.e. the absorber is isothermal at any point in time). Despite the varying volume of air in this process, the flow analysis is considered as an incompressible airflow due to prevalent low velocities much below a Mach number of 0.3 [17]. The Mach number is a dimensionless quantity and a measure of compressibility of flow representing the ratio of speed of an object moving through a fluid and the local speed of sound given by

$$\mathrm{M} = \frac{\mathrm{v}_{\mathrm{object}}}{\mathrm{v}_{\mathrm{sound}}} \tag{4}$$

where M is the Mach number in the medium, $\mathrm{v}_{\mathrm{object}}$ υ is the velocity of the source relative to the medium, and $\mathrm{v}_{\mathrm{sound}}$ υ is the speed of sound in the medium.

If M < 0.2-0.3 and the flow is (quasi)-steady and isothermal, compressibility effects will be small and a simplified incompressible flow model can be used. This implies that the density variation produced by the pressure and temperature variations is significantly small to be important. This is because the dynamic nature of the flow process represented by the square of the ratio of local flow velocity to speed of sound, U^2/V^2, known as the square of the Mach number, is much less than the ratio of inertia force to viscous force of the flow, ϱUL/μ, known as the Reynolds number. This condition for incompressibility of flow expressed as $M^2 << Re$ is satisfied in the flow analysis of the solar chimney.

Principles and theories governing natural free convection heat transfer are required for the determination of collector performance parameters. The effective performance of a solar chimney of this type is usually investigated through experimental data using high-precision apparatus and equipment. The absorbed solar radiation by the collector surface is transferred from both sides of the plate to air with the elimination of back insulation losses. In the course of analysis of this chimney-type solar collector, a number of assumptions were made to override these features such that the analyzed values of the collector correlates with the experimental values.

6. Solar insolation data at experimental setup location

The experimental setup was located at Nsukka, Nigeria, longitude 7° 23′ 45″ E and latitude 6° 51′ 24″ N [18], and the data acquisition method was adopted from the works of [9]. Solar data readings were taken on 23rd November at the location for analytical purposes. This implies that the day of the year is

$$I_n = 304 + 23 = 327 \tag{5}$$

Declination of that day is given by

$$\delta = 23.45 \sin\left[0.9863\left(284 + n\right)\right] = 20.8° \tag{6}$$

where δis *the declination*, ω is the hour angle and φ *is t*he *latitude*. The values of θ_z are tabulated in Table 1.

Solar time interval	7-8	8-9	9-10	10-11	11-12	12-1	1-2	2-3	3-4	4-5
Midpoint time	7.30	8.30	9.30	10.30	11.30	12.30	1.30	2.30	3.30	4.30
Hour angle	-67.5	-52.5	-37.5	-22.5	-7.5	7.5	22.5	37.5	52.5	67.5
Zenith angle	71.6	58.3	45.8	35.1	28.3	28.3	35.1	45.8	58.3	71.6

Table 1. Solar insolation data at experimental setup location

A sample of measured data for the month of November is given in Table 2 indicating the values of the total hourly solar radiation for all the 30 days of the month. This data was used as a case study with the assumption that insolation recorded for a particular month is approximately the same for the same month for every other year. This implies that insolation recorded in November 1975 is approximately the same as that recorded in November 2001.

http://dx.doi.org/10.5772/59423

Solar time	I_T (KJ/m^2)	I_b (KJ/m^2)	I_d (KJ/m^2)
7.30	1022.29	228.15	79.34
8.30	897.85	228.15	667.69
9.30	804.32	228.15	576.17
10.30	685.39	228.15	457.25
11.30	620.17	225.88	394.29
12.30	544.57	225.88	318.69
1.30	468.72	223.63	245.09
2.30	403.43	223.63	179.79
3.30	365.04	221.41	143.63
4.30	336.97	221.41	115.56

Table 2. Measured instantaneous values of solar insolation for the day 23rd November 1975

Table 3 shows the values of hourly insolation for 23rd November 2002 for which the values of beam and diffuse insolations above were deduced.

Time	7-8	8-9	9-10	10-11	11-12	12-1	1-2	2-3	3-4	4-5
I_T (KJ/m^2)	133.2	466.2	865.8	1287.6	1338.6	1420.8	1465.2	1332.0	976.8	532.8
I_b (KJ/m^2)	24.64	242.3	637.1	1062.1	1114.4	1199.2	11245.2	1107.6	747.8	307.8
I_d (KJ/m^2)	108.5	223.9	228.7	225.51	224.22	221.63	219.96	224.4	228.9	224.9

Table 3. Computed instantaneous values of hourly insolation for 23rd November 2002

Solar radiation components on a tilted collector are made up of the beam radiation component, the diffuse radiation component and the ground-reflected diffuse radiation components. Hence, the total hourly solar radiation on a collector surface is the summation of the three components:

$$I_c = I_{bc} + I_{dc} + I_{dgc} \tag{7}$$

where subscript c denotes solar radiation on the collector. For the case study, considering the collector being a vertical wall and no vegetation covering the ground, $\beta=90°$ and $\varrho=0.2$. Both sides of each wing are exposed to diffuse radiation, while only one side of the wings is exposed to direct beam radiation depending on the area factor receiving this direct radiation. Hence, the total radiation aimed at each wing of the collector is

$$I_{ci} = \forall I_b R_{bi} + 2\left[0.5I_d + 0.1\left(I_d + I_b\right)\right] = \left(\forall R_b + 0.2\right)I_b + 1.2I_d \tag{8}$$

where i is numbered subscripts 1, 2 and 3 denoting wing positions. The values are tabulated in Table 4.

Time	7-8	8-9	9-10	10-11	11-12	12-1	1-2	2-3	3-4	4-5
I_{c1} (KJ/m^2)	0.1783	0.5165	0.6529	0.5924	0.6480	0.6999	0.6653	0.6049	0.4958	0.3100
I_{c2} (KJ/m^2)	0.1659	0.5098	0.8013	1.0682	1.0714	1.1294	1.1991	1.1853	1.0189	0.5780
I_{c3} (KJ/m^2)	0.1376	0.3403	0.4675	0.6612	0.6723	0.6738	0.6413	0.9272	1.0420	0.8696
I_r (KJ/m^2)	0.4818	1.366	1.9217	2.2735	2.3917	2.5031	2.5057	2.7174	2.5567	1.8086

Table 4. Computed values of hourly insolation on each wing

7. Optical performance of glazing and absorption of solar radiation

Several optical properties (such as transmittance, reflectance and absorptance) of the glaze cover, most of which depend on the incident angle, affect the absorption of solar radiation. These optical properties in turn depend on the thickness of glazing and the refractive index and extinction coefficient of the glaze material.

Some of the radiation passing through the glaze and striking the absorber plate is reflected back to the cover system. However, not all of this radiation is lost since some of it is reflected back to the plate. The multiple reflections and absorptions between the plate and the cover is the greenhouse effect. To account for this greenhouse phenomenon, the actual fraction of incident radiation absorbed by the plate is called the transmittance-absorptance product ($\tau\alpha$). This was reasonably approximated by [19] as

$$\left(\tau\alpha\right) = A\left(\tau\right)\alpha_p \tag{9}$$

The constant A ranges from 1.01 to 1.02, but for conservativeness, 1.01 is preferred:

$$\left(\tau\alpha\right) = 1.01\left(\tau\right)\alpha_p \tag{10}$$

For transmittance of diffuse radiation, the effective incident angle θ_1 for vertical collectors is 59.5° for both ground and sky diffuse radiation. Hence, the effective refractive angle θ_2 of diffuse radiation from Snell's law is

http://dx.doi.org/10.5772/59423

$$\theta_2 = \sin^{-i}\left[\frac{n_1}{n_2}\left(\sin\theta_1\right)\right] = \sin^{-i}\left[\sin 59.5° / 1.526\right] = 34.4° \tag{11}$$

Likewise, the reflection components $r_{\perp}$ and $r_{\parallel}$ are evaluated from the equations below:

$$\left.\begin{aligned} r_{\perp} &= \frac{\sin^2\left(\theta_2 - \theta_1\right)}{\sin^2\left(\theta_2 + \theta_1\right)} = \frac{\sin^2\left(34.4 - 59.5\right)}{\sin^2\left(34.4 + 59.5\right)} = 0.181 \\ r_{\parallel} &= \frac{\tan^2\left(34.4 - 59.5\right)}{\tan^2\left(34.4 + 59.5\right)} = 0.001 \end{aligned}\right\} \tag{12}$$

The transmittance components are

$$\left.\begin{aligned} \tau_{\perp} &= \frac{\left(1 - \tau_{\perp}\right)}{\left(1 + \tau_{\perp}\right)} = \frac{1 - 0.181}{1 + 0.181} = 0.693 \\ \tau_{\parallel} &= \frac{\left(1 - \tau_{\parallel}\right)}{\left(1 + \tau_{\parallel}\right)} = \frac{1 - 0.001}{1 + 0.001} = 0.998 \end{aligned}\right\} \tag{13}$$

The average transmittance is $\tau_r = 0.5\left(\tau_{\perp} + \tau_{\parallel}\right) = 0.693 + 0.998 = 0.8455$

Accounting for cover absorptance,

$$\begin{aligned} \tau_a &= e^{-kL/\cos\theta_2} \\ &= e^{-0.0125/\cos 34.4} = 0.985 \end{aligned} \tag{14}$$

Hence, the resultant transmittance for diffuse radiation τ_d is determined from the following equation [19]:

$$\tau_d = \tau_r . \tau_a = 0.985\, x\, 0.8455 = 0.833 \tag{15}$$

Solar absorptance of the selective absorber plate $(\alpha)_p = 0.9$; hence, the transmittance-absorptance product for diffuse radiation is

$$\left(\tau\alpha\right)_d = 1.01\left(0.833\right)\left(0.9\right) = 0.757 \tag{16}$$

7.1. Absorption of radiation

Evaluating all necessary optical properties of the glass glazing, the amount of solar radiation actually absorbed by the collector can be easily deduced. The total incident radiation aimed at each wing of the collector is

$$I_{ci} = \forall I_b R_{bi} + 2\left[0.5I_d + 0.1\left(I_d + I_b\right)\right] \tag{17}$$

the total absorbed solar radiation of each wing is

$$S_i = (\tau\alpha)_b \forall I_b R_{bi} + 2(\tau\alpha)_b \left[0.5I_d + 0.1\left(I_d + I_b\right)\right] \tag{18}$$

$$= \left(\tau\alpha\right)_b \forall I_b R_{bi} + (\tau\alpha)_b \left[I_d + 0.2\left(I_d + I_b\right)\right] \tag{19}$$

The mean absorbed solar radiation, S, of the whole collector plate is evaluated by the relation

$$S = 1/3\left[S_1 + S_2 + S_3\right] \tag{20}$$

Applying the above expressions with other expressions for optical properties for calculating the absorbed radiation, the values calculated are tabulated as shown in Table 5.

Time	7-8	8-9	9-10	10-11	11-12	12-1	1-2	2-3	3-4	4-5
I_b (MJ/m^2)	0.0246	0.2423	0.0371	1.0621	1.1144	1.1992	1.2452	1.1076	0.7478	0.3078
I_d (MJ/m^2)	0.1086	0.2239	0.2287	0.2255	0.2242	0.2216	0.2200	0.2244	0.2290	0.2250
S_1 (MJ/m^2)	0.136	0.384	0.418	0.389	0.240	0.507	0.505	0.464	0.380	0.275
$\forall_1$	1	1	1	1	1	0.4260	0.1870	0.1010	0.0590	0.0320
R_{b1}	1.7480	0.8260	0.3940	0.1030	0.1400	0.3800	0.6540	1.0200	1.6200	2.993
$(\tau\alpha)_{b1}$	0.774	0.720	0.572	0.214	0.302	0.640	0.768	0.808	0.820	0.823
$(\tau\alpha)_{d1}$	0.757	0.757	0.700	0.757	0.757	0.757	0.757	0.757	0.757	0.757
S_2 (MJ/m^2)	0.124	0.377	0.593	0.793	0.797	0.840	0.889	0.873	0.743	0.516
$\forall_2$	1	1	1	1	1	1	1	1	1	1
R_{b2}	1.247	0.795	0.627	0.551	0.520	0.520	0.551	0.627	0.795	1.247
$(\tau\alpha)_{b2}$	0.691	0.709	0.722	0.730	0.733	0.733	0.730	0.722	0.709	0.691
$(\tau\alpha)_{d2}$	0.757	0.757	0.757	0.757	0.757	0.757	0.757	0.757	0.757	0.757
S_3 (MJ/m^2)	0.104	0.259	0.357	0.465	0.488	0.434	0.416	0.621	0.766	0.667
$\forall_3$	0.032	0.059	0.101	0.187	0.426	1	1	1	1	1
R_{b3}	2.993	1.620	1.020	0.654	0.380	0.140	0.103	0.394	0.826	1.748
$(\tau\alpha)_{b3}$	0.823	0.820	0.808	0.768	0.640	0.302	0.214	0.572	0.720	0.774
$(\tau\alpha)_{d3}$	0.757	0.757	0.757	0.757	0.757	0.757	0.757	0.757	0.757	0.757
S (MJ/m^2)	0.121	0.430	0.466	0.549	0.568	0.594	0.603	0.653	0.630	0.486

Table 5. Measured insolation data for each of the absorbers

http://dx.doi.org/10.5772/59423

7.2. The collector efficiency factor and the collector loss coefficient

Despite the unusual configuration of the tri-wing absorber plate, a section of it reduces to a vertical flat-plate collector over both sides of the plate without back insulation. This implies that a wing of the absorber can be treated as a flat-plate air heater with flow over both sides of the plate. To conform to the performance equation of a flat-plate collector, the configuration of the chimney collector is transformed to suit the equation. Criteria for the transformation are as follows:

1. The total area of the tri-wing absorber plate is equal to the total area of the flat absorber plate.
2. The height of the chimney collector is the same as the height of the resulting flat absorber plate.
3. The area of the circular inlet column of the chimney collector and the rectangular area inlet column of the resulting flat-plate collector are equal throughout the height of the collector.
4. The resulting flat-plate absorber is positioned within the rectangular column such that the flow is halved.
5. Size difference of the glass glazing of the two cases is neglected. The resulting flat-plate collector has an absorber plate 5.3m in height and 2.4m in breadth enclosed by a rectangular channel of glass glazing measuring 2.46m by 0.8587m in length and breadth. Thus, the flow width on either side of the plate is about 43cm.

8. Heat transfer and collector performance analysis

Considering a vertical absorber plate of one wing of the collector heated by insolation to a temperature T_p, a free convection boundary layer is formed [20, 21]. The boundary layer is such that at the wall of the plate, the velocity of air stream is zero. This increases to some maximum value and then decreases to zero due to free stream conditions, provided the gap between the plate and the cover is much greater than the boundary layer thickness.

From the prevailing conditions of the system, temperature $T=T_p$ at $y=0$, $T=T_\infty$ at $y=\delta$ and $\frac{dt}{dy}=0$ at $y=\delta$, a parabolic temperature function can be assumed to represent the temperature profile of the system with respect to y.

The expressions for the overall collector heat loss coefficient U_L and the collector efficiency factor F', which are very important performance parameters, were applied in the evaluation of useful energy rate extracted from the collector. To incorporate the flow rate and express the system energy equation using the collector inlet temperature, another performance parameter is introduced as the collector heat removal factor F_R. The collector heat removal factor is defined as the ratio of actual useful heat collector rate to useful heat collector rate attainable with the entire collector surface at the inlet fluid temperature. This is stated mathematically as

$$F_R = \frac{mC_p\left(T_o - T_1\right)}{A_c\left[S - U_L\left(T_1 - T_a\right)\right]} = \left[\frac{mC_p}{A_cU_L}\right]\left[1 - e^{-\frac{A_cU_L F}{mC_p}}\right] \tag{21}$$

Thus, the energy equation of the system becomes

$$Q_u = 2A_cF_R\left[S - U_L\left(T_1 - T_a\right)\right] \tag{22}$$

The efficiency of the whole collector system η defined as the ratio of the useful heat extracted from the collector Q_u to the total incident solar radiation on the collector is mathematically expressed as

$$\eta = \frac{Q_u}{A_cI_T} = 2F_R\left[\left(\tau\alpha\right)_c - \frac{U_L}{I_T}\left(T_1 - T_a\right)\right] \tag{23}$$

where $(\tau\alpha)$ is the effective transmittance-absorptance product of the collector glazing expressed by equation (24)

$$\left(\tau\alpha\right)_c = \frac{S_T}{I_T} \tag{24}$$

where T_1 and T_a are the collector's inlet and outlet temperatures, respectively.

9. Results and discussions

The derived expressions were utilized in evaluating the performance of the chimney, and the results were tabulated in Table 6. The outcome of the resulting parameters modelled from the analysis was graphically plotted to illustrate the performance efficiency of the chimney. This analysis is based on the use of a selective surface; in practice, the use of a non-selective absorbing surface with known properties is recommended for durability and economy.

Time	7.30	8.30	9.30	10.30	11.30	12.30	1.30	2.30	3.30	4.30
T_a (°C)	29.30	30.10	31.85	32.65	33.20	33.35	33.80	34.90	35.90	36.80
I_T (MJ/m^2)	0.1334	0.4662	0.8658	1.2876	1.3386	1.4208	1.4652	1.332	0.9768	0.5328
I_1(MJ/m^2)	0.121	0.340	0.466	0.549	0.568	0.594	0.603	0.653	0.630	0.486
S (MJ/m^2)	2.593	3.306	3.546	3.676	3.702	3.735	3.744	3.809	3.772	3.553
a h ($w/m^2\,°C$)	41.260	58.67	68.36	70.13	75.78	77.98	79.09	82.53	82.30	74.80
T_p (°C)	29.31	32.80	35.48	37.69	37.57	38.35	38.95	39.85	40.67	40.50
U_t (w/m^2°C)	13.95	14.12	14.25	14.35	14.37	14.41	14.45	14.50	14.56	14.60

http://dx.doi.org/10.5772/59423

Time	7.30	8.30	9.30	10.30	11.30	12.30	1.30	2.30	3.30	4.30
h_r $(w/m^2°C)$	0.6554	0.7252	0.7690	0.7980	0.8039	0.8150	0.8214	0.8380	0.8400	0.8105
F'	0.835	0.859	0.862	0.863	0.863	0.862	0.862	0.862	0.861	0.856
U_L $(w/m^2°C)$	6.100	7.116	7.395	7.711	7.754	7.819	7.848	7.959	7.933	7.640
T_F (°C)	31.70	38.66	42.94	50.32	46.24	47.26	47.90	48.31	49.82	47.88
U $(m/s)^{-1}$	0.261	0.360	0.407	0.255	0.436	0.446	0.450	0.464	0.459	0.421
m (kg/s)	0.384	0.518	0.577	0.353	0.612	0.623	0.628	0.644	0.637	0.588
Q_u(w)	227.71	751.25	1041.35	365.36	1275.77	1558.17	1374.99	1500.80	1448.91	1123.48
F_R	0.7670	0.7970	0.8024	0.7660	0.8048	0.8050	0.8047	0.8054	0.8035	0.797
T_t (°C)	31.53	38.30	42.48	50.05	45.71	45.41	47.34	48.71	49.24	47.40
$(\tau\alpha)_c$	0.9084	0.7293	0.5382	0.4264	0.4243	0.4181	0.4116	0.4902	0.6450	0.9122
H	0.577	0.444	0.332	0.079	0.263	0.303	0.260	0.311	0.410	0.582

Table 6. Results of modelled parameters from experimental analysis

The graph of temperatures versus diurnal hours, as shown in Figure 4, illustrates that peak values of the chimney air temperature are in the range 31.7 °C-50.32 °C compared with peak values of ambient air temperature in the range 26.20°C -28.30 °C. This gives a minimum temperature elevation of 3.4 °C and a maximum temperature elevation of 17.67 °C. It has been earlier stated that an effective design of the solar chimney is that which maintains the chimney air temperature consistently above the ambient air temperature.

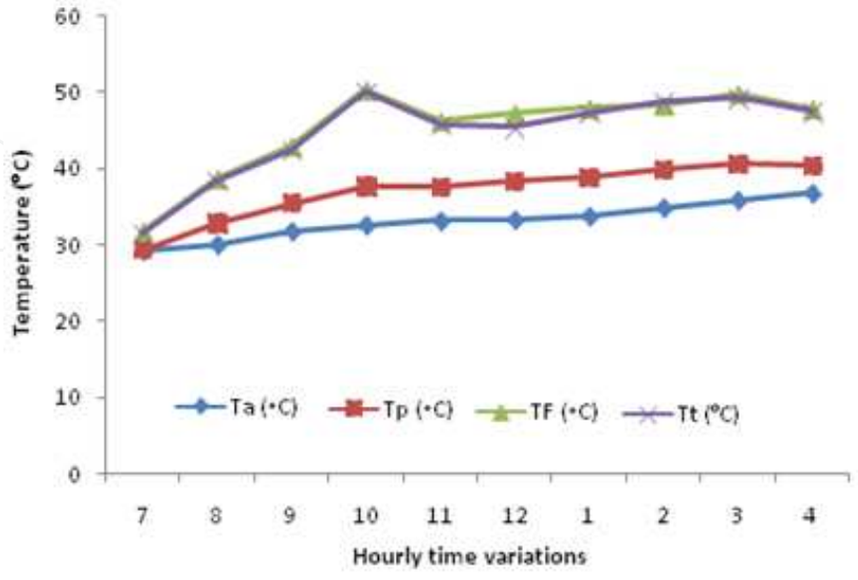

Figure 5. Diurnal variation of chimney and ambient temperatures

The graph showed that chimney air temperature is always within the range of absorber plate and glass cover temperatures. This indicated that the chimney air is heated by the collector plate which is at a higher temperature but loses heat to the glazing which is at a lower temperature.

Figure 5 shows the values of direct beam radiation R_b and diffuse radiation S for all hours of insolation on each wing. It is evident from the figure that the components of radiation are lower at near noon due to low values of R_b at this time. This is a result of the collector standing in a vertical position and the location near the equator. Highest components of direct beam radiation may be obtained for locations farther away from the equator. The diffuse solar radiation component absorbed by the collector will be evidently greater.

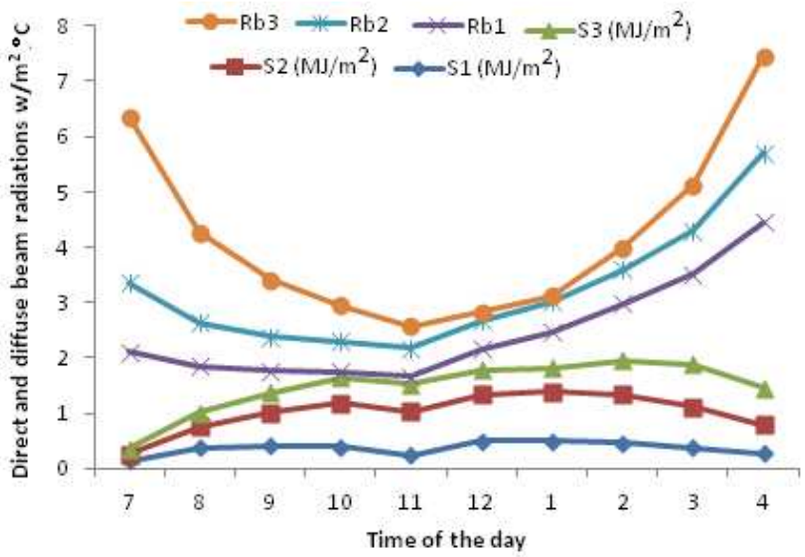

Figure 6. The values of direct beam radiation Rb for all hours of insolation on each wing

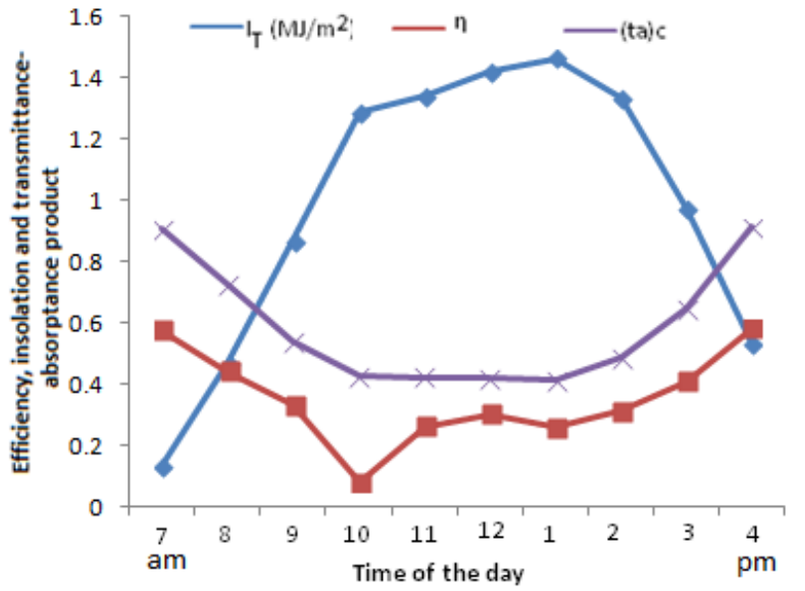

Figure 7. Graph of efficiency, insolation and transmittance-absorptance product

http://dx.doi.org/10.5772/59423

The graph of efficiency versus insolation shown in Figure 6 indicates that higher efficiencies of the collector are obtained during early and late hours despite high insolations available at near-noon hours. This is mainly due to lower values of the effective transmittance-absorptance product prevailing at near-noon hours.

10. Adaptation to wood drying

Mechanical wood drying processes have included forced air or fan drying or dehumidification processes using a kiln [22]. These processes involve very high operating costs to power the fan. High-rise solar chimneys had been widely used in solar updraft power plants (SUPP) to updraft heated air to the atmosphere; however, this heat can be redirected back to the room for the purpose of heating the room under natural convection. Applying this principle, depending on outside temperature and humidity, the solar heated air within the chimney can be conventionally forced back to the room space where lumbers were stacked by covering the top of the chimney from where the exhaust air escapes. By so doing, the hot air displaces the cooler air from the air duct causing hot air down-draft into the chamber, and the process repeats itself. The analyses of thermal exchange air conditioning, air circulation in drying products and drying efficiency are still under investigation.

11. Conclusion

From the computed parameters of the collector presented in the tables, it is observed that low variance is exhibited for U_t, U_L, F' and F_R. This indicates that the characteristics of the solar chimney are uniform over a wide range of operations. The result shows that buoyant airflow within the chimney is possible and the variation of air temperature elevation with insolation is minimal while the chimney has better efficiency at lower values of solar radiation. Thus, the aim of this work, which was to devise a method of analysis of thermal performance for this type of solar chimney, has been accomplished.

Nevertheless, a method of complete analytical evaluations that will give satisfactory results can be achieved by obtaining a table of correlation factor from experimental data values to analytical values of this kind.

Author details

R. S. Bello[1*], C. N. Ezebuilo[1], K. A. Eke[1] and T. A. Adegbulugbe[2]

*Address all correspondence to: segemi2002@yahoo.com

1 Federal College of Agriculture, Ishiagu, Nigeria

2 Federal College of Agriculture, Moor Plantation, Ibadan, Nigeria

References

[1] Hirunlabh, J. Study of natural ventilation of houses by a metallic solar wall under tropical climate. Renewable Energy 1999: Vol. 18 No. 1, pp. 109-119. http://en.wikipedia.org/wiki/Solar_chimney (assessed on September 2012).

[2] Shiv, L., Kaushik, S.C. and Bhargav, P.K. Solar chimney: A sustainable approach for ventilation and building space conditioning. International Journal of Development and Sustainability 2013: Vol. 2 No. 1, pp. 277-297.

[3] Gan, G. A parametric study of Trombe wall for passive cooling of buildings. Energy and Buildings 1998: Vol. 27, pp. 37-43.

[4] Bello, R. S. and Mohammed, A. S. Simulation of performance equations of passive integral solar water heating and storage system (ICS). Science Academy Transactions on Renewable Energy Systems Engineering and Technology (SATRESET) 2012: Vol. 2 No. 3 (September 2012 ISSN: 2046-6404). URL: http://www.sciacademypublisher.com/journals/index.php/SATRESET.

[5] Bello, R. S. and Odey, S. O. Development of hot water solar oven for low temperature thermal processes. Leonardo Electronic Journal of Practices and Technologies 2009: No. 14, 73-84 Romania. ISSN: 1583-1078. URL: www.lejpt.academicdirect.org/A14/073_084.pdf.

[6] Bello, R. S., Odey, S. O., Eke, K. A., Mohammed, A. S., Balogun, R. B., Okelola, O. and Adegbulugbe, T. A. Application of Asphalt bonded solar thermogenerator in small scale agroforesty based industry. In Elisha, B. Babatunde (Ed). Solar Radiation. Reijeka: InTech 2012. pp 459-484. ISBN: 978-953-51-0384-4. URL:http://www.intechopen.com/books/solar-radiation.

[7] Hirunlabh, J. New configurations of a roof solar collector maximizing natural ventilation. Building and Environment 2001: Vol. 36 No. 3, pp. 383-391.

[8] Bansal, N.K., Mathur, J. and Bhandari, M.S. Solar chimney for enhanced stack ventilation. Building and Environment 1993: Vol. 28 No. 3, pp. 373-377.

[9] Ong, K. S. A Mathematical Model of a Solar Chimney. Monash University Malaysia 46150 Petaling Jaya, Malaysia: 2001.

[10] Alter, L. The Trombe wall: Low tech solar design makes a comeback 2011. available at:http://www.treehugger.com/sustainable-product-design/the-trombe-wall-low-tech-solar-design-makes-a-comeback.html/ (assesses October 2012).

[11] Khedari, J. Ventilation impact of a solar chimney on indoor temperature fluctuation and air change in a school building. Energy and Buildings 2000: Vol. 32 No. 1, pp. 89-93.

[12] Zhai, X., Dai, Y. and Wang, R. Comparison of heating and natural ventilation in a solar house induced by two roof solar collectors. Applied Thermal Engineering 2005: Vol. 25 No. 5-6, pp. 741-757.

[13] Hirunlabh, J. Khedari, J. and Bunnag T. Experimental study of a roof solar collector towards the natural ventilation of new houses. Energy and Buildings 1997: Vol. 26 No. 2, pp. 159-164. International Journal of Development and Sustainability 2013: Vol. 2 No. 1, pp. 277-297. ISDS www.isdsnet.com 295.

[14] Ekechukwu, O. V. and Norton, B. Design and measured performance of a solar chimney for natural circulation solar-energy dryers. Renewable energy 1997: Vol. 10, pp. 81-90.

[15] Mathur, J. and Mathur, S. Summer-performance of inclined roof solar chimney for natural ventilation. Energy and Buildings 2006: Vol. 38 No. 10, pp. 1156-1163.

[16] Lee, K.H. and Strand, R.K. Enhancement of natural ventilation in buildings using a thermal chimney. Energy and Buildings 2009: Vol. 41 No. 6, pp. 615-621.

[17] Wikipedia. Mach number. 2014 http://en.wikipedia.org/wiki/Mach_number.

[18] Wikipedia. Nsukka. 2014 http://en.wikipedia.org/w/index.php?title=Nsukka&action=history.

[19] Duffie, J. A. and Beckman, W. A. Solar Energy Thermal Processes. John and Sons Pub NY. 2003.

[20] McAdams, W. H. Heat Transmission, 3rd edition. McGraw-Hill, New York 1954.

[21] Holman, J. P. Heat Transfer. National students' edition, McGraw-Hill, Inc 1976.

[22] Bello, R. S. Workshop Technology & Practice. Pub by Createspace 7290 B. Investment Drive Charl US. 2012. ISBN-13: 978-147-928-308-8. URL: https://www.createspace.com/3982311.

IntechOpen